



Cite this: *J. Anal. At. Spectrom.*, 2017, **32**, 1730

## Characterization of oxidized Ni-based superalloys by GD-OES

W. J. Nowak \*

In this work, the analysis of various high-temperature materials after oxidation using Glow Discharge Optical Emission Spectrometry (GD-OES) will be presented. The results of depth profiles of four Ni-based superalloys that form different oxide scales after oxidation at high temperatures will be shown. It was determined that GD-OES is a very flexible method allowing for analysis of different types of oxide scales formed on the alloys after operation. This method enables analysis of the oxides varying in chemical composition, as well as thickness (ranging between a few  $\mu\text{m}$  up to 150  $\mu\text{m}$ ). It will be shown that the GD-OES method is not only suitable for analysis of oxide scales, but also for studying protective coatings on a superalloy substrate, commonly used in the hot sections of gas turbines or jet engines. It was found that the GD-OES technique allows to obtain depth-resolved information with relatively good depth resolution at very thick layers, where other techniques fail due to *e.g.* sputtering time. The presence of precipitates and laterally inhomogeneous oxides additionally excludes other techniques with high lateral resolution. The results of GD-OES analysis will be confirmed by other analytical techniques, such as light optical microscopy (LOM) and scanning electron microscopy (SEM).

Received 23rd February 2017  
Accepted 12th April 2017

DOI: 10.1039/c7ja00069c

rsc.li/jaas

### 1. Introduction

Energy demand combined with requirements for environmental protection has led to an increase in Turbine Inlet Temperature (TIT) inside gas turbines. This causes the materials used in gas turbines to degrade due to high temperature oxidation. During exposure at high temperatures, oxidation products start to form at the interface between the alloy (coating) and the surrounding atmosphere. This effect leads to changes in the local chemical composition in the region below the oxide scale due to the consumption of the alloying elements during the reaction of the alloy with the environment. After a continuous oxide scale is formed, the reactants become separated and the oxidation rate is controlled by solid state diffusion through the oxide according to the mechanism described by Wagner.<sup>1</sup> Under thermal cyclic conditions the formed oxide scale tends to spall off resulting in a loss of wall thickness in the case of low-alloyed materials. In order to limit rapid oxidation, modern alloys, *e.g.* Ni-based superalloys, containing elements, such as Cr or Al, which form protective, slowly growing oxide scales (chromia and alumina scale, respectively) while exposed to high temperatures<sup>2-3</sup> are used. Taking into consideration the influence of Cr and Al on the mechanical properties of the alloys at room temperature, their content is limited. Therefore, many of the superalloys are classified as

marginal chromia or alumina formers.<sup>3</sup> Thus, to protect the alloys used in the hottest parts of the gas turbines against high temperature oxidation, special coatings, *e.g.*  $\beta$ -NiAl<sup>4,5</sup> or MCrAlY (M = Ni, Co) type coatings,<sup>6</sup> are commonly used.

To investigate the oxidation behavior of the materials used in the hot sections of gas turbines or jet engines under laboratory conditions, oxidation tests at an elevated temperature are performed. After oxidation the samples are commonly investigated by means of a number of analytical techniques, including X-ray Diffraction (XRD), Light Optical Microscopy (LOM), Scanning and Transmission Electron Microscopy (SEM/TEM), Mass Spectrometry (MS) and Optical Emission Spectrometry (OES). In the past few years, Glow Discharge Optical Emission Spectrometry (GD-OES) became a very popular method for investigating high-temperature materials after exposure to corrosive conditions.<sup>7</sup> Another advantage of the GD-OES technique is the possibility of measuring and detecting nearly all elements simultaneously. The latter allows for recording the depth profiles of unexpected elements.

The basis of GD-OES is that the measured surface is sputtered by plasma, layer by layer, and part of the sputtered atoms become excited in the plasma. Shortly after excitation, the atoms undergo disexcitation. During the latter process excess energy is emitted in the form of light with a given wavelength characteristic for each element. Measuring the intensity of the light with a given wavelength as a function of sputtering time allows for qualitative interpretation of the element distribution within the oxide scale and the regions below. The GD-OES profiles are commonly quantified by using the emission yield

Department of Materials Science, Faculty of Mechanical Engineering and Aeronautics, Rzeszow University of Technology, al. Powstańców Warszawy 12, 35-959 Rzeszow, Poland. E-mail: w.nowak@prz.edu.pl

concept, which also allows the conversion of time into the depth using a density model.<sup>8–10</sup> The GD-OES profile quantification is also possible by using the Relative Sensitivity Factors (RSFs).<sup>11</sup> It was shown in the papers published by the group of High-Temperature Corrosion and Corrosion Protection in Forschungszentrum Juelich that GD-OES analysis is a very useful method not only for investigating the overall chemical composition of oxide scales, but also for distributing elements such as C, B or S, which are difficult to investigate by means of conventional analytical methods like SEM/EDX due to their low atomic numbers.<sup>12–18</sup> Incorporation of other elements, such as zirconium<sup>19</sup> or yttrium,<sup>20</sup> into the oxide scale was successfully investigated using the GD-OES technique. Due to the limited spectral resolution of commercial spectrometers it is impossible to distinguish isotopes like <sup>16</sup>O and <sup>18</sup>O, which were used as markers during oxidation tests and successively measured by secondary neutral mass spectrometry (SNMS).<sup>21</sup> However, it is possible to effectively distinguish H and D *via* GD-OES,<sup>22</sup> which can also be used in a similar manner as <sup>16</sup>O and <sup>18</sup>O during oxidation tests. As previously described, the GD-OES technique is an excellent analytical method, however, its potential is not limited only to depth profiling. Shimizu *et al.*<sup>23</sup> successfully used GD-OES to prepare a sample for SEM observation. Therefore, GD-OES has a wide range of potential applications.

In this paper, a variety of applications of the GD-OES method in the high-temperature range will be presented. The results of the GD-OES depth profiles of different Ni-based superalloys and MCrAlY type coatings will be presented. The quantification procedure will be shortly described as well. Finally, the GD-OES depth profile of a real gas turbine component after operation will be presented. All GD-OES analyses will be combined with the results of “standard” analytical methods, such as LOM or SEM.

## 2. Experimental

In order to present the potential application of the GD-OES technique in the high-temperature oxidation range, four different alloys were chosen and investigated. The nominal chemical compositions of these alloys are shown in Table 1.

Rectangular specimens with 20 × 10 × 2 mm dimensions were cut from these materials. The surfaces were ground on SiC paper up to 1200 grit and then ultrasonically cleaned in ethanol prior to oxidation.

Isothermal oxidation tests were performed using a TGA 92-16.18 Setaram thermobalance at 1050 °C up to 50 hours in laboratory air. The heating rate was 90 K min<sup>-1</sup>, the cooling rate 10 K min<sup>-1</sup> and the gas flow rate 2 dm<sup>3</sup> h<sup>-1</sup>.

Additionally, a part from a gas turbine blade was investigated by means of GD-OES and LOM. The analysed component comes from the cooling channel of the gas turbine blade after operating for around 10 000 hours. Inside the cooling channel, the blade is aluminized.

Glow discharge optical emission analysis (GD-OES) was performed on samples after oxidation and before cross-section preparation. The GD-OES depth profiles were obtained using a GD Profiler HR (Horiba Jobin Yvon). All analyses were conducted under the same sputtering conditions, *i.e.* with an argon pressure of 700 Pa and 30 W power using an anode made of copper with a 4 mm diameter. The argon used in the analysis had a very high purity of 6 N. The wavelengths used for the measured elements are listed in Table 2. The method enables measuring the depth profiles with a relatively high sputtering rate (depth up to 200 μm sputtered within 2500 seconds). Quantification of GD-OES depth profiles was performed according to the procedure similar to that proposed by Pfeifer *et al.*,<sup>11</sup> instead of the procedure based on emission yields described *e.g.* by Nelis *et al.*,<sup>8</sup> Gonzalez-Gago *et al.*<sup>9</sup> or Weiss.<sup>10</sup> Such a quantification procedure has been chosen due to the fact that the wavelength for oxygen detection is 130 nm, which causes problems with quantification *via* the matrix-independent method as reported by Gonzalez-Gago *et al.*<sup>9</sup> Moreover, the matrix-independent quantification method would require a calibration material with a different matrix. Since all alloys investigated in the present study are Ni-based, the use of matrix-specific calibration is preferred.

Prior to cross-section preparation, the oxidized specimens were cut in the middle, sputtered with a very thin gold layer using cathodic evaporation, electrolytically coated with nickel and mounted in resin. Metallographic cross-sections of the

Table 1 Nominal chemical composition of the investigated alloys (given in wt%)

Name of the alloy	Elements (wt%)													
	Ni	Cr	Ta	Co	Mo	W	Al	Ti	Zr	B	Fe	Y	Re	C
IN 792	BASE	12.50	4.00	8.90	1.90	4.00	3.40	4.00	0.02	0.02	0.20	—	—	0.08
PWA 1483	BASE	12.00	5.00	9.00	1.90	3.80	3.60	4.20	0.03	0.01	—	—	—	0.07
MCrAlY	BASE	17.00	—	25.00	—	—	10.00	—	—	—	—	0.40	1.50	—
Rene 80	BASE	14.00	—	9.50	4.00	4.00	3.00	5.00	0.03	0.02	—	—	—	0.16

Table 2 Wavelengths used for detection of certain elements

Element	O	C	S	B	Co	Ni	Re	Ta	Ti	Y	Mo	Al	Cr	W
Wavelength (nm)	130	156	181	209	229	341	345	363	365	377	386	396	425	429

alloy after oxidation, as well as under the as-cast conditions, were prepared by a series of grinding and polishing steps, the final of which was fine polishing in SiO<sub>2</sub> suspension with 0.25 μm granulation. The cross-sections were analyzed using LOM and SEM.

### 3. Results and discussion

#### a. Laboratory testing

According to the oxidation map introduced by Giggins and Pettit,<sup>3</sup> the alloys based on Ni–Cr–Al can form different types of oxide scales depending on their chemistry. In Fig. 1 superimposition of three studied Ni-based superalloys into the oxidation map is presented. One can observe that IN 792 and PWA 1483 can be classified as marginal alumina-forming alloys, whereas the MCrAlY type alloy is a typical alumina-forming alloy. However, the measured mass changes (Fig. 2) and calculated instantaneous

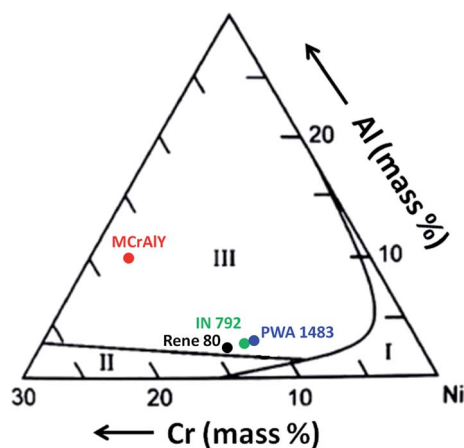


Fig. 1 Oxidation map of Ni–Cr–Al alloys<sup>3</sup> showing areas of various types of oxide scale formation as a function of Cr and Al contents in alloys at 1000–1100 °C: (I) NiO-forming alloys, (II) Cr<sub>2</sub>O<sub>3</sub>-forming alloys, and (III) Al<sub>2</sub>O<sub>3</sub>-forming alloys. Cr and Al contents of IN 792, PWA 1483, Rene 80 and MCrAlY are superimposed.

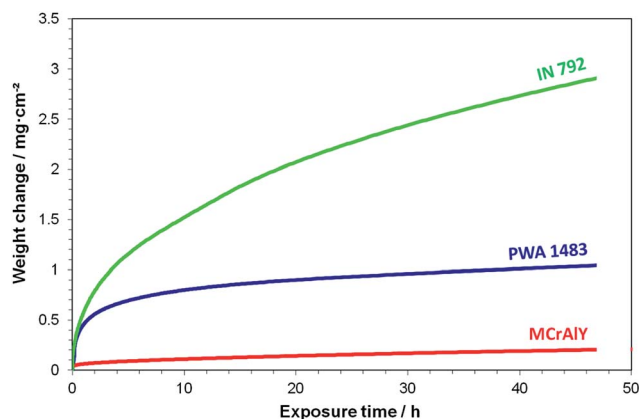


Fig. 2 Mass changes obtained for the studied alloys during isothermal exposure to laboratory air at 1050 °C for 50 h.

oxidation rate plots  $k'_w$  (Fig. 3) for the studied alloys show that all of them have different oxidation rates. The instantaneous oxidation rate constants  $k'_w$  were calculated according to the procedure described by Quadackers *et al.*<sup>24</sup> The obtained  $k'_w$  values differ substantially between the studied alloys, even between IN 792 and PWA 1483 although both are classified to be alumina formers on the basis of their Cr and Al contents (see Fig. 1). To investigate the reason for such a difference, further studies, such as GD-OES depth profiling and SEM analysis, have been performed.

The GD-OES depth profiles illustrating the intensities of light emitted by certain elements as a function of sputtering time are shown in Fig. 4. On the basis of these profiles the oxide scale composition and the depletion regions in the alloys below the oxide scale can only be qualitatively estimated. However, after the quantification process described below, the “raw” results of GD-OES depth profiling can be recalculated into the concentration of elements as a function of sputtering time using the so-called Relative Sensitivity Factors (RSFs).<sup>11</sup> The RSFs for element X were calculated using the following equation:

$$\text{RSF}_X = \left( \frac{c_X}{c_A} \right) \left( \frac{I_A}{I_X} \right) \quad (1)$$

where:  $c_X$  – atomic concentration of element X,  $c_A$  – atomic concentration of basic element A (matrix),  $I_X$  – measured light intensity of element X, and  $I_A$  – measured light intensity of element A being the matrix (in the present case Ni).

The RSF for oxygen can be calculated, after assuming a M<sub>2</sub>O<sub>3</sub> oxide type formation according to the following equation:

$$\frac{I_X \times \text{RSF}_X}{I_O \times \text{RSF}_O} = \frac{2}{3} \quad (2)$$

where:  $I_X$  – measured light intensity of element X,  $\text{RSF}_X$  – calculated RSF for element X,  $I_O$  – measured light intensity for oxygen, and  $\text{RSF}_O$  – calculated RSF for oxygen.

Concentration can be calculated using the following equation:

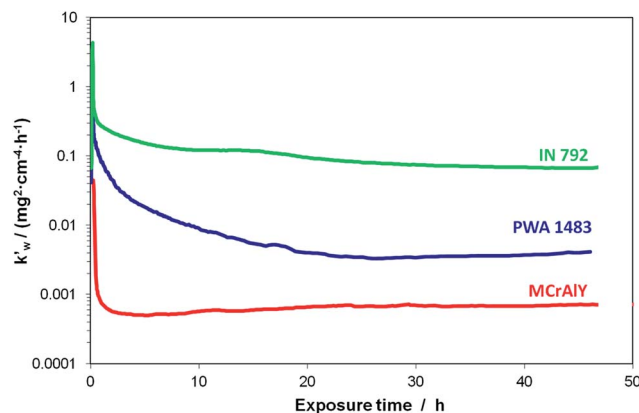


Fig. 3 Instantaneous apparent parabolic rate constant  $k'_w$  obtained for the studied alloys during isothermal exposure to laboratory air at 1050 °C for 50 h.  $k'_w$  was calculated using data from Fig. 2 in accordance with the procedure described in ref. 24.

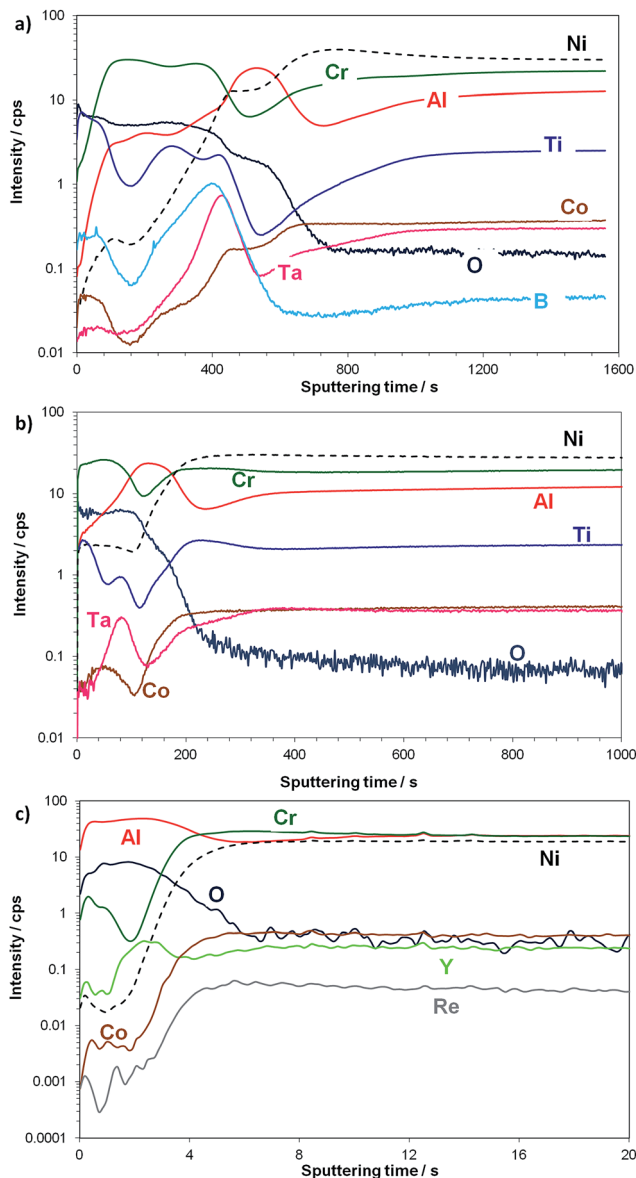


Fig. 4 "Raw" GD-OES depth profiles illustrating the intensity of light for the given elements as a function of sputtering time determined for: (a) IN 792, (b) PWA 1483 and (c) MCrAlY after isothermal oxidation performed at 1050 °C for 50 hours in laboratory air.

$$c_X = \frac{(I_X \times \text{RSF}_X)}{\left( \sum_{i=1}^n I_i \times \text{RSF}_i \right) + I_O \times \text{RSF}_O} \quad (3)$$

where:  $I_X$  – measured light intensity of element X,  $\text{RSF}_X$  – calculated RSF for element X,  $i$  –  $i$ -th alloying element in the  $n$ -element alloy,  $I_O$  – measured light intensity for oxygen, and  $\text{RSF}_O$  – calculated RSF for oxygen.

Using RSFs, the concentration profiles can be calculated according to the following procedure. The concentration of the elements in the bulk alloy was determined by means of inductively-coupled plasma optical emission spectrometry (ICP-OES) for major alloying elements, inductively-coupled plasma mass spectrometry (ICP-MS) for minor alloying elements and

combustion analysis for non-metallic elements (C, S, and O). The RSF for a given element was determined by the correlation between the light intensity measured on a non-exposed material and its concentration derived from the previously described chemical composition measurement. The RSF for oxygen was determined under the assumption that the alloy forms  $M_2O_3$  type oxides ( $Al_2O_3$ ) and using only one reference sample, which was the oxidized MCrAlY type alloy itself. The light intensities of the elements used in the calculations were taken from the time, where a  $M_2O_3$  type oxide was formed in multilayered oxide scales. Moreover, a linear correlation between the light intensity and the concentration was assumed. Such an attempt leads to semi-quantitative results, which enable the estimation of the stoichiometry of formed oxides. It is known that species such as  $H_2O$  or  $OH$  make it difficult to quantify oxygen. However, since the semi-quantitative results obtained in the present study are satisfactory for estimating oxide stoichiometry, their influence was neglected. Converting sputtering time into depth is also a problematic issue due to the fact that in multilayered samples different layers might (and they most probably will) exhibit different sputtering rates. Furthermore, the presence of light elements in the oxide scale causes a problem with such conversion by means of a simple density model used in the emission yield model. However, recent innovation in GD-OES equipment, namely Differential Interferometry Profiling (DIP) developed by Horiba Jobin Yvon<sup>25</sup> is intended to overcome these problems.

An alternative method is to use the concept of matrix-independent emission yields.<sup>8–10</sup> The correspondence between both methods can be established by considering the definition of a RSF, eqn (1), and the definition of the corresponding emission yield, see ref. 10. Under certain assumptions, it is also possible to calculate the depth beneath the surface as a function of sputtering time.

Fig. 5 shows the GD-OES depth profiles after quantification. On the basis of these profiles one can make conclusions about the stoichiometry of the formed oxides. The obtained results presented in Fig. 5 reveal that a multiphase oxide scale was formed on IN 792 and PWA 1483.

In the outer part of the oxide scale grown on IN 792 (Fig. 5(a)), enrichment of Ti is observed (0 to 100 s), below which the scale is rich in Cr (100 to 400 s). Below that, a peak of Cr, co-enrichment of Ti and Ta are present (400 to 450 s). Two plateaus are visible in the oxygen profile. The oxygen content indicates that the first plateau illustrates the outer part of the oxide scale (oxygen content of about 60 at%) and the second shows the region of internal oxidation (oxygen content of about 20–30 at% with simultaneously higher Ni and Co contents from the alloy matrix). In the region of the second oxygen plateau, a relatively high peak of aluminum is observed (450 to 650 s). The latter indicates the presence of a zone containing internally oxidized aluminum. Below the aluminum peak, a depletion zone pertaining to this element can be found (650 to 850 s). This depletion is caused by Al-consumption during  $Al_2O_3$  formation.

The GD-OES analysis performed on PWA 1483 after oxidation (Fig. 5(b)) showed qualitatively similar profiles to IN 792, namely outer Ti enrichment, below which enrichment of Cr and

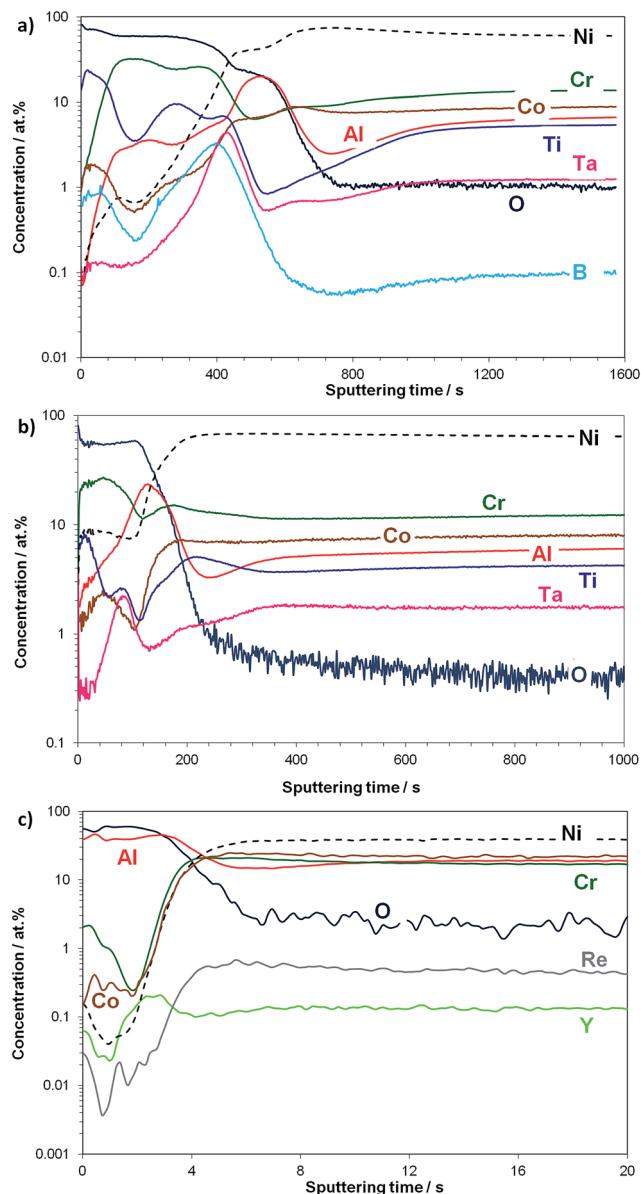


Fig. 5 Quantified GD-OES depth profiles showing the atomic concentration of the given elements as a function of sputtering time determined for: (a) IN 792, (b) PWA 1483 and (c) MCrAlY after isothermal oxidation performed at 1050 °C for 50 hours in laboratory air.

co-enrichment of Ti and Ta can be observed. At the oxide/alloy interface, an Al peak can be found. However, in this case, the second plateau is not observed in the oxygen profile. This indicates the formation of a continuous alumina sub-layer. In the case of internal oxidation, a second plateau with a lower oxygen intensity/concentration is expected due to the fact that a matrix is entrapped at the internal oxidation zone between the internal oxide precipitates. Therefore, the signal coming from the oxygen is lower compared to that detected in the continuous oxide layer. As previously shown for IN 792, depletion of aluminum is visible under the alumina scale. It must be emphasized that the sputtering time illustrating the oxide scale

region finishes after 200 s, whereas in the previous case it was 700 s including the internal oxidation zone.

Finally, the GD-OES depth profile of MCrAlY (Fig. 5(c)) indicated that the oxide scale consists of relatively pure alumina (high enrichment of aluminum in the outer part of the oxide scale). Below the alumina scale, enrichment of yttrium is observed. The sputtering time representing the oxide scale zone reaches 5 s. From this the formation of a thin and protective alumina scale can be concluded.

For a better description of the oxidized alloys, the cross-sectional analysis by means of SEM has been performed. Fig. 6 shows the SEM images of the studied alloy cross-sections after oxidation at 1050 °C for 50 hours in laboratory air. The obtained results confirmed the data obtained by GD-OES. Moreover, the types of the formed oxides were identified.

Fig. 6(a) presents the microstructure of the oxide scale formed on IN 792 during 50 h oxidation at 1050 °C in air. The SEM/EDX analysis revealed that the oxide scale consists of  $\text{TiO}_2$  in the outer part of the oxide scale. Below the latter a relatively thick region of  $\text{Cr}_2\text{O}_3$  is present. Near the oxide scale/alloy interface formation of  $\text{TiTaO}_4$  is observed, as well as the zone of internal aluminum oxidation. The morphology of the oxide scale formed on IN 792 is very similar to the oxide scale grown on another Ni-based alloy with a similar chemical composition, *i.e.* Rene 80. The oxidation behavior of Rene 80 at 1050 °C was investigated by *e.g.* Jalowicka *et al.*<sup>16</sup> or Nowak *et al.*<sup>26</sup> In both studies, Rene 80 formed an oxide scale similar to the one described here for IN 792. Moreover, Jalowicka<sup>16</sup> explained the formation of a chromium rich oxide scale on Rene 80 by Ti-doping, which increases the chromia growth rate, thereby suppressing the formation of a continuous alumina scale. In this work, both marginal alumina-forming alloys, namely IN 792 and PWA 1483, also contain about 4 wt% Ti. Moreover, IN 792 contains 4 wt% Ta, while PWA contains 5 wt% Ta. It was determined by Jalowicka *et al.*<sup>16</sup> that the addition of Ta leads to the formation of  $\text{TiTaO}_4$  which should suppress the flux of Ti through the oxide scale. However, as shown in Fig. 6(b), the addition of 5 wt% Ta enables the formation of a nearly continuous  $\text{TiTaO}_4$  layer on PWA 1483, while on IN 792  $\text{TiTaO}_4$  is present in the form of precipitates (Fig. 6(a)). Therefore, it might be speculated that the formation of a  $\text{TiTaO}_4$  layer helped create a continuous sub-layer of alumina on PWA 1483, whereas the formation of a continuous sub-layer of alumina cannot be observed on IN 792 after 50 hours of exposure. Another explanation for the different oxidation behaviors of IN 792 and PWA1483 can be the difference in alloy microstructures. As shown in Fig. 7, IN 792 is a polycrystalline material, whereas PWA1483 is a single crystal. Therefore, Ti-transport to the surface through grain boundaries is increased in the case of IN 792. Moreover, the higher carbon content in IN 792 might result in tying up Ta in the form of carbides in the case of IN 792, which in turn might result in a less Ta content available for  $\text{TiTaO}_4$  formation.

The microstructure of the oxide scale observed on MCrAlY *via* SEM confirmed the formation of a relatively pure, thin and protective alumina scale with about 2  $\mu\text{m}$  thickness. Near the oxide scale/alloy interface, formation of Y-rich precipitates is

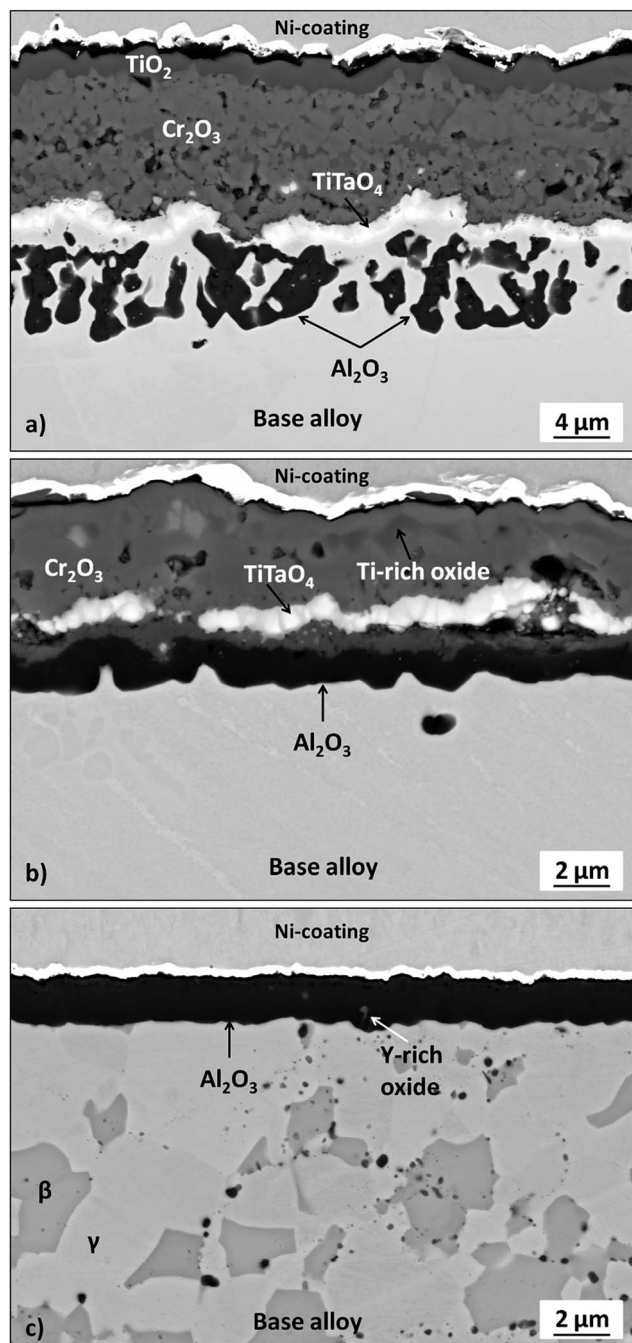


Fig. 6 SEM/BSE images of: (a) IN 792, (b) PWA 1483 and (c) MCrAlY cross-sections after isothermal oxidation at 1050 °C for 50 hours in laboratory air.

observed. The formation of such precipitates was previously observed in the literature by, *e.g.*, Gil *et al.*<sup>27</sup>

### b. Component after service

As described in the previous chapter, the GD-OES technique can be effectively used to characterize the samples exposed to laboratory conditions. However, as this chapter will show, GD-OES analysis can be successively performed on real components of gas turbines after operation. Various oxidation-

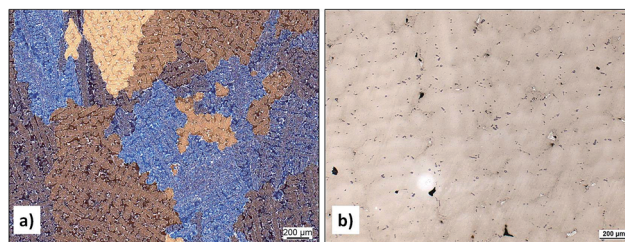


Fig. 7 LOM images illustrating the microstructure of: (a) IN 792 and (b) PWA1483 under the as-received conditions. Both surfaces were etched for better visualization of their microstructure. Different colors represent separate grains.

resistant coatings are applied on the base alloys, used as a construction material, in order to protect them against aggressive hot gases. The outer part of a turbine blade is covered mainly with MCrAlY type alloys deposited using plasma spraying methods.<sup>20,28</sup> On the other hand, in the cooling channels, application of the coatings by means of plasma spraying is impossible due to geometrical limitations. Therefore, the chemical vapor deposition (CVD) technique is commonly used to produce aluminide coatings.<sup>29</sup> Fig. 8 presents the cross-sectional image of a part of the turbine blade from the cooling channel. It can be seen that the aluminide coating is applied on the base alloy, which in this case is Ni-based superalloy Rene 80, the chemical composition of which is given in Table 1. Between the aluminide coating and the base material an interdiffusion zone is present. This zone contains the so-called

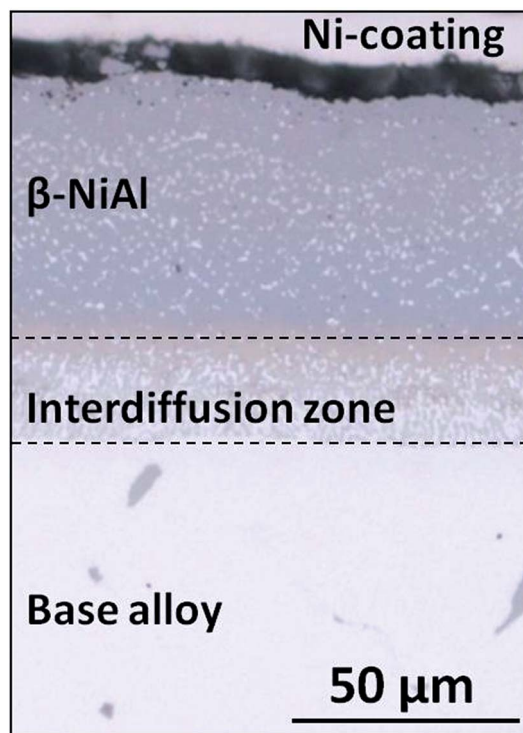


Fig. 8 Light optical microscopic image of the cross-section across a cooling channel of a turbine blade after approximately 10 000 hours of operation.

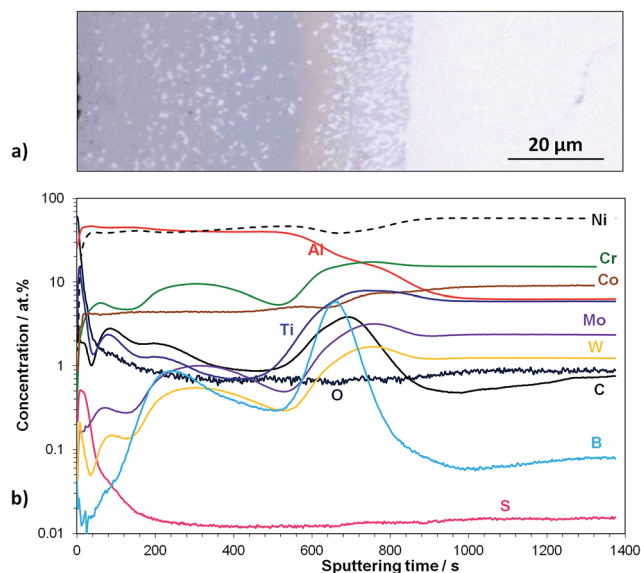


Fig. 9 Comparison of: (a) microstructure (optical metallographic image) and (b) GD-OES depth profile of aluminized Rene 80 used in the cooling channel of a gas turbine blade after approximately 10 000 hours of service.

topologically close-packed (TCP) phases.<sup>12</sup> The GD-OES depth profile presented in Fig. 9(b) reveals that the outer part of the coating consists of  $\beta$ -NiAl. Below the aluminide coating, an interdiffusion zone is present, in which a co-enrichment of Ti, Mo and W is visible. Moreover, enrichment of carbon is observed. This might indicate the formation of carbides within the interdiffusion zone. Such carbide formation in the aluminized Ni-based alloy has already been found and described by Pillai *et al.*<sup>12</sup> Just below the aluminide coating an enrichment of boron is found. Boron is present in Rene 80 and it was already determined that during the exposure of unmodified Rene 80, boron diffuses outwards, forms a stable mixed oxide,  $\text{BCrO}_3$ , and becomes depleted in the bulk alloy.<sup>14</sup> However, as found by Nowak *et al.*,<sup>15</sup> formation of a continuous alumina sub-layer suppresses boron depletion. It can be speculated that the aluminide coating might also hinder outward boron diffusion. Therefore, a boron peak is observed below the coating. Alternatively, boron can form a compound with another element, such as Cr, the activity of which is increased by Al-diffusion from the coating, as determined by Chyrkin *et al.*<sup>30</sup> Beneath the oxide scale formed on the coating, an enrichment of sulfur was found. The presence of sulfur in the aluminide coating was not expected. Therefore, such enrichment suggests the formation of sulfides below the oxides. Sulfur, most probably, comes from the exhaust fumes, because sulfur is intentionally added to the fuel to avoid its sedimentation. Measurement of the crater depth of the profile presented in Fig. 9(b) reveals that it is possible to measure the depth profile obtained by GD-OES up to 120 μm, which is not possible using other depth profiling techniques, such as plasma-SIMS or SNMS. Therefore, it can be concluded that GD-OES is an excellent method for investigating a wide range of coatings and oxide thicknesses.

## 4. Summary and conclusions

In this work, GD-OES analysis of oxidized Ni-based superalloys is presented. It is shown that profiling of oxides and coating with various thicknesses and chemistry is possible. From all the presented results it can be concluded that:

- GD-OES allows for analysis of oxide scales with various thicknesses, from about 2 μm up to about 120 μm;
- Studying different types of oxide scales, such as  $\text{Al}_2\text{O}_3$  or  $\text{Cr}_2\text{O}_3$  or, as in most cases in this work, multilayered systems is possible;
- Due to the high sputtering rate, GD-OES allows fast analysis with reasonable depth resolution;
- Analysis of light elements, *e.g.* boron, is possible, using the GD-OES technique as opposed to *e.g.* SEM, where it is not very easy. Thus, GD-OES studies combined with other “standard” analytical methods help to fully describe the samples;
- Analysis of nearly every element enables the determination of non-expected elements in the samples, such as sulfur from the fuel that forms sulfides below the oxide scale as shown in this work;
- Presenting intensities as a function of sputtering time is commonly accepted and might give valuable information concerning what happens in the sample during oxidation, however, it is possible to quantify the results;
- A simple quantification based on the ratio model, used in this study, gives semi-quantitative information enabling the estimation of the types and stoichiometry of the formed oxides,
- If more accurate quantification is demanded, quantification based on the emission yield model should be applied. In this work, quantification using the emission yield model was impossible due to the fact that the wavelength used for oxygen detection was 130 nm, which leads to problems with oxygen quantification,
- In both aforementioned methods, namely the ratio model and emission yield model, conversion of sputtering time into depth is problematic and the uncertainty of such estimation might be significant,
- Finally, it was shown that not only samples manufactured in laboratories, but also real components used in the stationary gas turbines can be successfully analyzed by GD-OES.

## Acknowledgements

The majority of the results were obtained in the Institute of Energy and Climate Research (IEK-2) in Forschungszentrum Juelich, Germany. Prof. W. J. Quadackers and Dr D. Naumenko are gratefully acknowledged for fruitful discussion and help with interpreting the results. The author is grateful to colleagues in the Institute for Energy and Climate Research (IEK-2) of the Forschungszentrum Juelich GmbH for carrying out the oxidation experiments (H. Cosler, R. Mahnke and A. Kick), light optical microscopy analysis (V. Gutzeit and J. Bartsch) and SEM analysis (Dr E. Wessel, Dr D. Grüner). Many thanks to Dr Patrick Chapon from Horiba Jobin Yvon for discussion and expertise in GD-OES. Financial support from the

European Union (Collaborative Project: FP7-239349 with acronym: H2-IGCC) is also gratefully acknowledged.

## Notes and references

- C. Wagner, Reaktionstypen bei der Oxydation von Legierungen, *Z. Elektrochem.*, 1959, **63**, 772–782.
- R. Prescott and M. J. Graham, The Formation of Aluminum Oxide Scales on High-Temperature Alloys, *Oxid. Met.*, 1992, **38**(3/4), 233–254.
- C. S. Giggins and F. S. Pettit, Oxidation of Ni–Cr–Al Alloys Between 1100° and 1200 °C, *Solid State Sci.*, 1971, **118**(11), 1782–1790.
- M. J. Pomeroy, Coatings for gas turbine materials and long term stability issues, *Mater. Des.*, 2005, **26**, 223–231.
- K. H. Stern, *Metallurgical and Ceramic Protective Coatings*, Chapman and Hall, 2–6 Boundary Row, London SE1 8HN, UK, 1996.
- K. Yuan, R. Eriksson, R. L. Peng, X.-H. Li, S. Johansson and Y.-D. Wang, Modelling of microstructural evolution and lifetime prediction of MCrAlY coatings on nickel based superalloys during high temperature oxidation, *Surf. Coat. Technol.*, 2013, **232**, 204–215.
- T. Nelis, Glow Discharge as a Tool for Surface and Interface Analysis, *Appl. Spectrosc. Rev.*, 2006, **41**, 227–258.
- T. Nelis and R. Payling, *Practical Guide to Glow Discharge Optical Emission Spectrometry*, Royal Society of Chemistry, Cambridge, UK, 2003.
- C. Gonzalez-Gago, P. Smid, T. Hofmann, C. Venzago, V. Hoffmann and W. Gruner, The use of matrix-specific calibrations for oxygen in analytical glow discharge spectrometry, *Anal. Bioanal. Chem.*, 2014, **406**, 7473–7482.
- Z. Weiss, Calibration methods in glow discharge optical emission spectrometry: a tutorial review, *J. Anal. At. Spectrom.*, 2015, **30**, 1038–1049.
- J. P. Pfeifer, H. Holzbrecher, W. J. Quadackers and J. Speier, Quantitative analysis of oxide films on ODS\*-alloys using MCs+SIMS and e-beam SNMS\*\*, *J. Anal. Chem.*, 1993, **346**, 186–191.
- R. Pillai, A. Chyrkin, D. Grüner, W. Nowak, W. J. Quadackers, N. Zheng and A. Kliewe, Carbides in an aluminised single crystal superalloy: tracing the source of carbon, *Surf. Coat. Technol.*, 2016, **288**, 15–24.
- A. Chyrkin, R. Pillai, H. Ackermann, H. Hattendorf, S. Richter, W. Nowak, D. Grüner and W. J. Quadackers, Modeling carbide dissolution in alloy 602 CA during high temperature oxidation, *Corros. Sci.*, 2015, **96**, 32–41.
- A. Jalowicka, W. Nowak, D. J. Young, V. Nischwitz, D. Naumenko and W. J. Quadackers, Boron Depletion in a Nickel Base Superalloy Induced by High Temperature Oxidation, *Oxid. Met.*, 2015, **83**(3–4), 393–413.
- W. Nowak, A. Jalowicka, V. Nischwitz, D. Gruner, D. Naumenko and W. J. Quadackers, Effect of oxide scale composition on boron depletion of Ni-base superalloys, *Mater. Corros.*, 2017, **68**(2), 171–185.
- A. Jalowicka, W. Nowak, D. Naumenko, L. Singheiser and W. J. Quadackers, Effect of nickel base superalloys composition on oxidation resistance in SO<sub>2</sub> containing, high pO<sub>2</sub> environments, *Mater. Corros.*, 2014, **65**(2), 178–187.
- P. Huczowski, T. Olszewski, M. Schiek, B. Lutz, G. R. Holcomb, V. Shemet, W. Nowak, G. H. Meier, L. Singheiser and W. J. Quadackers, Effect of SO<sub>2</sub> on oxidation of metallic materials in CO<sub>2</sub>/H<sub>2</sub>O-rich gases relevant to oxyfuel environments, *Mater. Corros.*, 2014, **65**(2), 121–131.
- A. Jalowicka, W. J. Nowak, D. Naumenko and W. J. Quadackers, Effect of SO<sub>2</sub> Addition on Air Oxidation Behavior of CM247 and CMSX-4 at 1050 °C, *J. Met.*, 2016, **68**, 2776–2785.
- P. Huczowski, S. G. Gopalakrishnan, W. Nowak, H. Hattendorf, R. Iskandar, J. Mayer and W. J. Quadackers, Effect of Zr-content on the morphology and emissivity of surface oxide scales on FeCrAlY alloys, *Adv. Eng. Mater.*, 2016, **18**, 711–720.
- E. Hejrani, D. Sebold, W. J. Nowak, G. Mauer, D. Naumenko, R. Vassen and W. J. Quadackers, Isothermal and cyclic oxidation behavior of free standing MCrAlY coatings manufactured by high-velocity atmospheric plasma spraying, *Surf. Coat. Technol.*, 2017, **313**, 191–201.
- W. J. Quadackers, A. Elshner, W. Spier and K. Nickel, Composition and growth mechanisms of alumina scales on FeCrAl-based alloys determined by SNMS, *Appl. Surf. Sci.*, 1990, **52**, 271–287.
- Y. Hatano, J. Shi, N. Yoshida, N. Futagami, Y. Oya and H. Nakamura, Measurement of deuterium and helium by glow-discharge optical emission spectrometry for plasma-surface interaction studies, *Fusion Eng. Des.*, 2014, **87**, 1091–1094.
- K. Shimizu and T. Mitani, *New Horizons of Applied Scanning Electron Microscopy, Springer Series in Surface Sciences*, ISBN 978-3-642-03159-5, Springer-Verlag, Berlin, Heidelberg, 2010.
- W. J. Quadackers, D. Naumenko, E. Wessel, V. Kochubey and L. Singheiser, Growth rates of alumina scales on FeCrAl alloys, *Oxid. Met.*, 2004, **61**, 17–37.
- S. Richard, J.-P. Gaston, O. Acher and P. Chapon, Glow discharge spectroscopy method and system for measuring *in situ* the etch depth of a sample, US Patent No. US 2017/0045457 A1, 2017.
- W. J. Nowak, P. Wierzba, D. Naumenko, W. J. Quadackers and J. Sieniawski, Water vapour effect on high temperature oxidation of superalloy Rene 80, *Postępy Technol. Masz. Urzadzen*, 2016, **40**, 41–52.
- A. Gil, D. Naumenko, R. Vassen, J. Toscano, M. Subanovic, L. Singheiser and W. J. Quadackers, Y-rich oxide distribution in plasma sprayed MCrAlY-coatings studied by SEM with a cathodoluminescence detector and Raman spectroscopy, *Surf. Coat. Technol.*, 2009, **204**, 531–538.
- W. Nowak, D. Naumenko, G. Mor, F. Mor, D. E. Mack, R. Vassen, L. Singheiser and W. J. Quadackers, Effect of processing parameters on MCrAlY bondcoat roughness

- and lifetime of APS-TBC systems, *Surf. Coat. Technol.*, 2014, **260**, 82–89.
- 29 K. L. Choy, Chemical vapour deposition of coatings, *Prog. Mater. Sci.*, 2003, **48**, 57–170.
- 30 A. Chyrkin, W. G. Sloof, R. Pillai, T. Galiullin, D. Gruner, L. Singheiser and W. J. Quadackers, Modelling compositional changes in nickel base alloy 602 CA during high temperature oxidation, *Mater. High Temp.*, 2015, **32**, 102–112.